AXISYMMETRIC RESPONSES OF THERMOPIEZOELECTRIC FINITE CYLINDER

Yasothorn Sapsathiarn[1], Panupong Boonphennimit[2], Jaroon Rungamornrat[3], and Teerapong Senjuntichai[4*]

[1] Department of Civil and Environmental Engineering, Faculty of Engineering, Mahidol University, Nakornpathom, Thailand, e-mail: Yasothorn.Sap@mahidol.ac.th

[2] Department of Civil Engineering, Faculty of Engineering, Chulalongkorn University, Bangkok, Thailand, e-mail: panupong.boon1987@gmail.com

[3] Department of Civil Engineering, Faculty of Engineering, Chulalongkorn University, Bangkok, Thailand, e-mail: Jaroon.R@chula.ac.th

[4,*] Department of Civil Engineering, Faculty of Engineering, Chulalongkorn University, Bangkok, Thailand, e-mail: Teerapong.S@eng.chula.ac.th (Corresponding author)

Received Date: December 17, 2013

Abstract

This paper is concerned with theoretical treatment of transient responses of finite thermopiezoelectric cylinder under axisymmetric mechanical, electrical and thermal loading. The analytical general solutions for axisymmetric deformations of a thermopiezoelectric medium are obtained in terms of series of Bessel and modified Bessel functions of the first kind. A boundary-value problem corresponding to a finite solid thermopiezoelectric cylinder with electrically impermeable boundary condition under applied axisymmetric electromechanical loading and temperature change is solved by expanding the applied load in terms of Fourier-Bessel series. Accuracy of the present numerical solution scheme is confirmed by comparing with existing transient solution of an elastic cylinder. To portray the salient features of the coupling transient responses of finite solid thermopiezoelectric cylinders, selected numerical results are presented for displacements, stresses and temperature distributions inside the cylinders subjected to applied traction together with prescribed temperature at the lateral curve surface of the cylinder.

Keywords: Axisymmetric problems, Finite cylinders, Thermal stress, Thermopiezoelectricity, Transient response.

Introduction

Piezoelectric materials have a wide range of engineering applications as sensors and actuators due to their inherent coupling electro-mechanical phenomena. In the field of civil engineering, piezoelectric materials have been extensively used for structural vibration control, structural health monitoring and adaptive (smart) structures [1, 2]. Under working conditions, piezoceramic sensors/actuators could experience severe temperature variations. For the development and design of piezoelectric elements suitable for practical applications under various temperature ranges, fundamental understanding of transient responses of piezoelectric devices under combined mechanical, electric and thermal loading is needed.

The mathematical framework and techniques used in the modeling of physical phenomena in piezoelectric media have been developed continuously since the discovery of such materials. Early studies, such as those by Mindlin [3], Chen [4], and Deeg [5], addressed some fundamental problems related to mechanics of piezoelectric materials. Parton and Kudryavtsev [6] presented the theoretical foundation of electroelastic governing equations and solutions for a variety of problems of linear piezoelectricity. Among several types of piezoelectric actuator/sensor elements, a solid cylindrical shape is widely used in practical applications. Several studies have been conducted in the past to

investigate electroelastic response of piezoelectric solid element. For instance, studies of electroelastic field in a long and finite solid piezoelectric cylinder under electromechanical loading were presented by Rajapakse and Zhou [7] and Senjuntichai *et al*. [8] respectively.

It is well known that thermal loading has significant impact on responses of piezoelectric components or systems operating at severe heating environments. Fundamental understanding and capability to accurately predict such temperature-dependent behavior are, as a result, crucial in the design procedure to ensure safety and integrity throughout their lifespan. However, the study of thermopiezoelectric elements has received limited attention when compared to piezoelectric elements. Ashida and Tauchert [9] investigated temperature, displacement, stress and electric fields of a finite circular piezoelectric disk subjected to axisymmetric loading, and also presented general solutions for a three dimensional thermopiezoelectric solid of class 6 mm. Tanigiwa and Ootao [10] employed Airy's stress function and Laplace integral transforms to derive the exact solution for transient temperature field of a two-layered, hollow, thermopiezoelectric cylinder under axisymmetric heating.

Based on the above introduction and review of the literature, it is clear that the understanding of thermopiezoelectric solid cylinder is crucial for piezoelectric sensors/actuators applications. According to our knowledge, a rigorous study of thermo-electro-mechanical behavior of a finite solid thermopiezoelectric cylinder has not appeared in the literature. The main objective of the present paper is thus to conduct a comprehensive analysis of a finite solid cylinder of piezoelectric material of crystal class 6 mm under axisymmetric electromechanical and thermal loading. The outcomes from the present work are useful for understanding the salient features of themopiezoelectric finite cylinder subjected to thermo-electro-mechanical loading, and could be served as benchmark analytical solutions for the verification of versatile numerical procedures such as finite element method (FEM) and boundary element method (BEM). The method outlined in the present work for finite solid thermopiezoelectric cylinders can also be extended to study transient thermopiezoelectric problems involving hollow and composite cylinders with finite length.

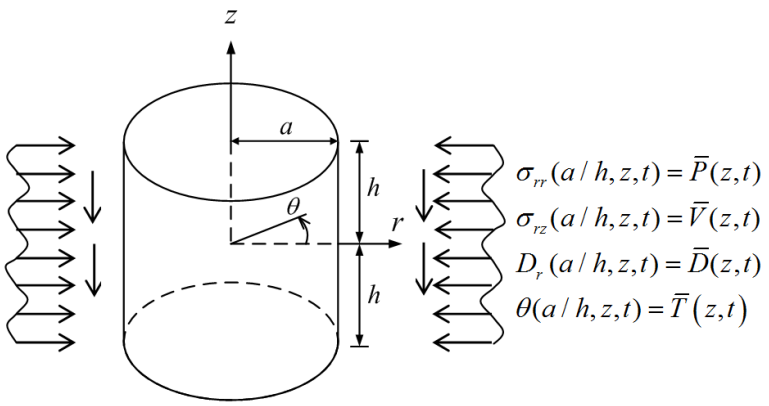

Figure 1**.** A finite solid thermopiezoelectric cylinder and corresponding reference coordinate systems.

Governing Equations and General Solutions

Consider a linear thermopiezoelectric finite solid cylinder of length 2*h* and radius *a* as shown in Figure 1. A cylindrical coordinate system (r,θ, z) is used in the analysis with the z-axis along the axis of symmetry of a cylinder (Figure 1). The cylinder is made of a linear, transversely isotropic thermopiezoelectric material of a special class 6mm. The linear

constitutive relations for thermopiezoelectric materials can be derived by considering the first and the second laws of thermodynamics (see Ikeda [11] for a detailed derivation). The constitutive equations for linear thermopiezoelectric materials that are transversely isotropic or poled along the *z*–axis can be expressed as [6]

$$\sigma_{rr} = c_{11}\varepsilon_{rr} + c_{12}\varepsilon_{\theta\theta} + c_{13}\varepsilon_{zz} - e_{31}E_z - \lambda_{11}\theta \tag{1a}$$

$$\sigma_{\theta\theta} = c_{12}\varepsilon_{rr} + c_{11}\varepsilon_{\theta\theta} + c_{13}\varepsilon_{zz} - e_{31}E_z - \lambda_{11}\theta \tag{1b}$$

$$\sigma_{zz} = c_{13}\varepsilon_{rr} + c_{13}\varepsilon_{\theta\theta} + c_{33}\varepsilon_{zz} - e_{33}E_z - \lambda_{33}\theta \tag{1c}$$

$$\sigma_{rz} = 2c_{44}\varepsilon_{rz} - e_{15}E_r \tag{1d}$$

$$D_r = 2e_{15}\varepsilon_{rz} + \in_{11} E_r + p_1\theta \tag{1e}$$

$$D_z = e_{31}\varepsilon_{rr} + e_{31}\varepsilon_{\theta\theta} + e_{33}\varepsilon_{zz} + \in_{33} E_z + p_3\theta \tag{1f}$$

$$S = \lambda_{11}\varepsilon_{rr} + \lambda_{11}\varepsilon_{\theta\theta} + \lambda_{33}\varepsilon_{zz} + p_1E_r + p_3E_z + \alpha\theta \tag{1g}$$

$$h_r = K_{11}e_r \;; \quad h_z = K_{33}e_z \tag{1h}$$

where σ_{ij} and ε_{ij} denote the components of stress and strain component respectively; D_i and E_i denote electric displacement vector and electric field vector respectively; θ denotes the temperature change from the reference temperature θ_0; S denotes the entropy density; e_i and h_i denote the temperature gradient and heat flux vector respectively; c_{11}, c_{12}, c_{13}, c_{33} and c_{44} are elastic constants under zero or constant electric field; e_{13}, e_{33} and e_{15} are piezoelectric constants; and $\in_{11}$ and $\in_{33}$ are dielectric constants under zero or constant strain; and p_k, K_{ij} and λ_{ij} denote the pyroelectric constants, coefficients of heat conduction and temperature-stress coefficients respectively. In addition, α is a material constant defined as $\alpha = \rho C_v / \theta_0$ where ρ is the mass density and C_v is the specific heat at constant volume.

The field equations for a three-dimensional linear thermopiezoelectric material undergoing axially symmetric deformations about the z-axis can be expressed as [6]

$$\frac{\partial\sigma_{rr}}{\partial r} + \frac{\partial\sigma_{rz}}{\partial z} + \frac{\partial\sigma_{rr} - \sigma_{\theta\theta}}{r} = 0; \quad \frac{\partial\sigma_{rz}}{\partial r} + \frac{\partial\sigma_{zz}}{\partial z} + \frac{\sigma_{rz}}{r} = 0 \tag{2a}$$

$$\frac{\partial D_r}{\partial r} + \frac{\partial D_z}{\partial z} + \frac{D_r}{r} = 0; \quad \frac{\partial h_r}{\partial r} + \frac{\partial h_z}{\partial z} + \frac{h_r}{r} = -\theta_0\frac{\partial S}{\partial t} \tag{2b}$$

Relations between electric field - electric potential (E_i - φ) and temperature gradient - temperature change (e_i - θ) are given by

$$E_r = -\frac{\partial\varphi}{\partial r}; \; E_z = -\frac{\partial\varphi}{\partial z}; \; e_r = -\frac{\partial\theta}{\partial r} \;; \quad e_z = -\frac{\partial\theta}{\partial z} \tag{3}$$

In view of Equation (1)-(3) and the classical strain–displacement relations in elasticity, along with additional assumptions that the velocity gradient is negligible and the electric field is quasi-static, the governing equations of a thermopiezoelectric material undergoing axisymmetric deformations about the *z*–axis can be expressed as

$$c_{11}\left(\frac{\partial^2}{\partial r^2}+\frac{1}{r}\frac{\partial}{\partial r}\right)u_r-c_{11}\frac{u_r}{r^2}+c_{44}\frac{\partial^2 u_r}{\partial z^2}+\left(c_{13}+c_{44}\right)\frac{\partial^2 u_z}{\partial r\partial z}+\left(e_{15}+e_{31}\right)\frac{\partial^2\varphi}{\partial r\partial z}-\lambda_{11}\frac{\partial\theta}{\partial r}=0 \tag{4a}$$

$$\left(c_{13}+c_{44}\right)\frac{\partial}{\partial z}\left(\frac{\partial u_r}{\partial r}+\frac{u_r}{r}\right)+c_{44}\frac{\partial^2 u_z}{\partial r^2}+c_{33}\frac{\partial^2 u_z}{\partial z^2}+c_{44}\frac{1}{r}\frac{\partial u_z}{\partial r}+e_{15}\left(\frac{\partial^2\varphi}{\partial r^2}+\frac{1}{r}\frac{\partial\varphi}{\partial r}\right)$$
$$+e_{33}\frac{\partial^2\varphi}{\partial z^2}-\lambda_{33}\frac{\partial\theta}{\partial z}=0 \tag{4b}$$

$$\left(e_{15}+e_{31}\right)\frac{\partial}{\partial z}\left(\frac{\partial u_r}{\partial r}+\frac{u_r}{r}\right)+e_{15}\left(\frac{\partial^2 u_z}{\partial r^2}+\frac{1}{r}\frac{\partial u_z}{\partial r}\right)+e_{33}\frac{\partial^2 u_z}{\partial z^2}-\in_{11}\left(\frac{\partial^2\varphi}{\partial r^2}+\frac{1}{r}\frac{\partial\varphi}{\partial r}\right)$$
$$-\in_{33}\frac{\partial^2\varphi}{\partial z^2}+p_3\frac{\partial\theta}{\partial z}+p_1\left(\frac{\partial\theta}{\partial r}+\frac{\theta}{r}\right)=0 \tag{4c}$$

$$\frac{K_{11}}{K_{33}}\left(\frac{\partial^2\theta}{\partial r^2}+\frac{1}{r}\frac{\partial\theta}{\partial r}\right)+\frac{\partial^2\theta}{\partial z^2}=\frac{\theta_0\alpha}{K_{33}}\frac{\partial\theta}{\partial t} \tag{4d}$$

At this stage, it is convenient to nondimensionalize all field variables. For example, the coordinates r and z and the displacements u_r and u_z are nondimensionalized by h (half length of the cylinder); the stresses and elastic constants are nondimensionalized by c_{11}; the electric displacements and piezoelectric constants are nondimensionalized by e_{33}; and the temperature-stress coefficients are nondimensionalized by λ_{11}. All parameters are replaced by non-dimensional quantities but the previous notations will be used for convenience.

The Laplace transform of a function $\phi(r,z,t)$ with respect to a time t and its inverse formula are defined by [12]

$$\tilde{\phi}(r,z,s)=\int_0^\infty \phi(r,z,t)e^{-st}dt \tag{5}$$

$$\phi(r,z,t)=\frac{1}{2\pi i}\int_{\beta-i\infty}^{\beta+i\infty}\tilde{\phi}(r,z,s)e^{st}ds \tag{6}$$

where s is the Laplace transform parameter and $i=\sqrt{-1}$. In addition, β is a sufficiently large real number.

It is evident that the three governing field equations (4a)–(4c) are fully coupled whereas the governing equation for the temperature change (Equations (4d)) is independent of the elastic displacement and the electric potential. By applying the Laplace transform to Equations (4d), the following solution of temperature change (θ) in the Laplace domain can be obtained.

$$\tilde{\theta}(r,z,s)=\sum_{p=0}^{\infty}A_p I_0\left(\frac{\chi_p r}{\delta}\right)\cos\left(\vartheta_p z\right)+\sum_{q=0}^{\infty}E_q{}' J_0\left(\frac{\mu_q r}{\delta}\right)\cosh\left(\eta_q z\right) \tag{7}$$

where $\chi_p = \sqrt{(\vartheta_p)^2 - s}$; $\eta_q = \sqrt{(\mu_q)^2 + s}$, and $\vartheta_p, \chi_p, \eta_q, \mu_q, A_p$ and E_q (p, q = 0, 1, 2, … ∞) are arbitrary functions to be determined; I_n is a modified Bessel function of the first kind of the n^{th} order; and J_n is a Bessel function of the first kind of the n^{th} order [13].

To solve the coupled system of equations (4a)–(4c), the elastic displacement u_r, u_z and the electric potential φ are represented by four potential functions ψ_1, ψ_2, ψ_3 and ψ_4 in the following forms [9]

$$u_r = \frac{\partial}{\partial r}(\psi_1 + \psi_2 + \psi_3 + \psi_4) \tag{8a}$$

$$u_z = \frac{\partial}{\partial z}(l_{11}\psi_1 + l_{12}\psi_2 + l_{13}\psi_3 + l_{14}\psi_4) \tag{8b}$$

$$\varphi = \frac{\partial}{\partial z}(l_{21}\psi_1 + l_{22}\psi_2 + l_{23}\psi_3 + l_{24}\psi_4) \tag{8c}$$

where l_{1i} and l_{2i} $(i = 1, 2, 3, 4)$ are unknown constant to be determined.

Solutions of displacements and electric potential can be obtained by substituting Equations (8a)-(8c) into Equations (4a)-(4c) and applying the Laplace transform. It can be shown that the corresponding solutions for the Laplace transforms of displacements and electric potential of the solid cylinder can be expressed as

$$\begin{aligned}\tilde{u}_r(r,z,s) = {} & 2\sum_{i=1}^{3} A_{0i} r + \sum_{i=1}^{3}\sum_{m=1}^{\infty} \upsilon_{im}\left[A_{im} I_1(\upsilon_{im} r)\right]\cos\left(\frac{\upsilon_m z}{\gamma_i}\right) - \sum_{i=1}^{3}\sum_{n=1}^{\infty} \xi_n\left[E_{in} J_1(\xi_n r)\right]\cosh\left(\frac{\xi_n z}{\gamma_i}\right) \\ & + \sum_{p=1}^{\infty}\frac{\chi_p}{\delta}\left[A_{4p} I_1\left(\frac{\chi_p r}{\delta}\right)\right]\cos(\vartheta_p z) - \sum_{q=1}^{\infty}\frac{\mu_q}{\delta}\left[E_{4q} J_1\left(\frac{\mu_q r}{\delta}\right)\right]\cosh(\eta_q z)\end{aligned} \tag{9a}$$

$$\begin{aligned}\tilde{u}_z(r,z,s) = {} & -4\sum_{i=1}^{3}\frac{l_{1i}}{\gamma_i} A_{0i} z + \sum_{i=1}^{3} l_{1i}\sum_{m=1}^{\infty}\frac{\upsilon_m}{\gamma_i}\left[-A_{im} I_0(\upsilon_m r)\right]\sin\left(\frac{\upsilon_m z}{\gamma_i}\right) \\ & + \sum_{i=1}^{3} l_{1i}\sum_{n=1}^{\infty}\frac{\xi_n}{\gamma_i}\left[E_{in} J_0(\xi_n r)\right]\sinh\left(\frac{\xi_n z}{\gamma_i}\right) \\ & - l_{14}\sum_{p=1}^{\infty}\vartheta_p\left[A_{4p} I_0\left(\frac{\chi_p r}{\delta}\right)\right]\sin(\vartheta_p z) + l_{14}\sum_{q=1}^{\infty}\eta_q\left[E_{4q} J_0\left(\frac{\mu_q r}{\delta}\right)\right]\sinh(\eta_q z)\end{aligned} \tag{9b}$$

$$\begin{aligned}\tilde{\varphi}(r,z,s) = {} & -4\sum_{i=1}^{3}\frac{l_{2i}}{\gamma_i} A_{0i} z + \sum_{i=1}^{3} l_{1i}\sum_{m=1}^{\infty}\frac{\upsilon_m}{\gamma_i}\left[-A_{im} I_0(\upsilon_m r)\right]\sin\left(\frac{\upsilon_m z}{\gamma_i}\right) \\ & + \sum_{i=1}^{3} l_{2i}\sum_{n=1}^{\infty}\frac{\xi_n}{\gamma_i}\left[E_{in} J_0(\xi_n r)\right]\sinh\left(\frac{\xi_n z}{\gamma_i}\right) \\ & - l_{14}\sum_{p=1}^{\infty}\vartheta_p\left[A_{4p} I_0\left(\frac{\chi_p r}{\delta}\right)\right]\sin(\vartheta_p z) + l_{24}\sum_{q=1}^{\infty}\eta_q\left[E_{4q} J_0\left(\frac{\mu_q r}{\delta}\right)\right]\sinh(\eta_q z)\end{aligned} \tag{9c}$$

where υ_m, ξ_n are constants; $\chi_p, \vartheta_p, \mu_p, \eta_p, A_{0i}, A_{im}, E_{in}$ $(i = 1, 2, 3)$ and A_{4p}, E_{4q} are a set of arbitrary functions. The parameters γ_i appearing in Equations (9) are the characteristic root of the materials.

The stresses, strains, electric fields and electric displacements corresponding to Equations (9a)–(9c) can be obtained from the classical strain–displacement relations in elasticity, Equations (1) and (3). To facilitate the solution of boundary-value problems, the general solutions for displacements, stresses, etc. are expressed as sum of five parts: (a) the first part denoted by superscript "0" corresponds to non-series terms; (b) the second part, denoted by a superscript „1", corresponds to the series of the modified Bessel function associated with l_{1i} and l_{2i} $(i=1,2,3)$; (c) the third part, denoted by a superscript „2", corresponds to the series of the Bessel function associated with l_{1i} and l_{2i} $(i=1,2,3)$; (d) the fourth part, denoted by a superscript „3", corresponds to the series of the modified Bessel function associated with l_{14}, l_{24} and the temperature field; and (e) the last part corresponds to the series of the Bessel function associated with l_{14} , l_{24} and the temperature field, and it is denoted by superscript „4".

Boundary-Value Problem of Finite Thermopiezoelectric Cylinder

The general solutions derived in the preceding sections are employed in this section for the analysis of a finite solid thermopiezoelectric cylinder subjected to axisymmetric prescribed traction $\bar{P}(z,t)$ and $\bar{V}(z,t)$, prescribed electric displacement $\bar{D}(z,t)$ and prescribed temperature $\bar{T}(z,t)$, on the lateral curved surface as shown in Figure 1. The top and bottom end surfaces are assumed to be traction-free, electrically impermeable [5] and zero heat flux. In the present study, the boundary conditions are given by

$$\sigma_{rr}(\frac{a}{h},z,t)=\bar{P}(z,t);\ \ \sigma_{rz}(\frac{a}{h},z,t)=\bar{V}(z,t)\ \text{for}\ 0<z<1 \tag{10a}$$

$$D_r(\frac{a}{h},z,t)=\bar{D}(z,t);\ \ \theta(\frac{a}{h},z,t)=\bar{T}(z,t)\ \text{for}\ 0<z<1 \tag{10b}$$

$$\sigma_{zz}(r,\pm 1,t)=0;\ \ \sigma_{zr}(r,\pm 1,t)=0\ \text{for}\ 0<r<a/h \tag{10c}$$

$$D_z(r,\pm 1,t)=0;\ \ h_z(r,\pm 1,t)=0\ \text{for}\ 0<r<a/h \tag{10d}$$

A linear algebraic equation system can be established to determine the arbitrary functions appearing in Equations (7) and (9) by applying appropriate boundary conditions. It can be shown that the general solution of temperature field that satisfies the boundary condition $h_z(r,\pm 1,t)=0$ is given by

$$\tilde{\theta}(r,z,s)=\sum_{p=0}^{\infty}\left[A_p I_0\left(\frac{\chi_p}{\delta}r\right)\right]\cos\left(\vartheta_p z\right) \tag{11}$$

where $\vartheta_p=p\pi$ for $p=0,1,2,...$

In order to apply the boundary condition $\theta(a/h,z,t)=\bar{T}(z,t)$, it is necessary to express $\bar{T}(z,t)$ in terms of identical functions of z (see Equation (11)). Introducing the Fourier cosine series expansion for the prescribed temperature in the Laplace domain as

$$\tilde{T}(z,s)=\frac{T_{10}}{2}+\sum_{p=1}^{\infty}T_{1p}\cos\left(\vartheta_p z\right) \tag{12}$$

where $T_{10}=2\int_0^1\cos\left(\vartheta_p z\right)dz$ and $T_{1p}=2\int_0^1 T_1(s,z)\cos\left(\vartheta_p z\right)dz$.

By applying the Laplace transform to thermal boundary conditions in Equations (10a) and (10d), together with the series in Equation (11), the arbitrary constants χ_p, η_q, μ_q and A_p can be determined. In addition, the potential functions $\tilde{\psi}_4$ can be expressed as

$$\tilde{\psi}_4 = \sum_{p=1}^{\infty} A_{4p} I_0(\chi_p r / \lambda\ ) \cos(\vartheta_p z_4) \tag{13}$$

where $A_{4p} = \dfrac{\lambda_{11}}{\left[c_{11}(\chi_p / \lambda\ )^2 - M_4(\vartheta_p)^2 \right]} A_p = \dfrac{\lambda_{11}}{\varpi} A_p$.

Next, the procedure for consideration of mechanical and electrical boundary conditions is illustrated. Consider, for example, the boundary condition $\sigma_{zz}(r, \pm 1, t) = 0$ at the top and bottom end surfaces of a cylinder. In order to satisfy the boundary condition, $\upsilon_{im} = m\pi\gamma_i$. Therefore, $\tilde{\sigma}_{zz}(r, \pm 1, s) = 0$ can be reduced to $\tilde{\sigma}_{zz} = \tilde{\sigma}_{zz}^0 + \tilde{\sigma}_{zz}^2 + \tilde{\sigma}_{zz}^3$. In addition, let

$$E_{in} J_1\left(\xi_{in} \frac{a}{h} \right) = 0 \tag{14}$$

From the above equation (14), the value of $\xi_{in} = \xi_{1n} = \xi_{2n} = \xi_{3n} = \xi_n$ can be determined, and $\tilde{\sigma}_{zz}^1$ can be expressed as

$$\tilde{\sigma}_{zz}^1 = \sum_{n=1}^{\infty} \sum_{i=1}^{3} (-1)^n \left(n\pi\gamma_i \right)^2 \left(c_{13} - \frac{c_{33} l_{1i}}{(\gamma_i)^2} - \frac{e_{33} l_{2i}}{(\gamma_i)^2} \right) A_{in} I_0(n\pi\gamma_i r) \tag{15}$$

Expanding functions $I_0\left(n\pi\gamma_i r\right)$ in terms of function $J_0\left(\xi_n r\right)$

$$I_0(n\pi\gamma_i r) = c_{I00} + \sum_{j=1}^{\infty} c_{I0j} J_0(\xi_j r) \tag{16a}$$

$$c_{I00} = \frac{2}{b^2} \int_0^{a/h} r I_0\left(n\pi\gamma_i r\right) dr\ ;\ \ c_{I0j} = \frac{2}{b^2 \left[J_0(\xi_j r) \right]^2} \int_0^{a/h} r J_0(\xi_j r) I_0(n\pi\gamma_i r) dr \tag{16b}$$

The function $\tilde{\sigma}_{zz}^1$ then becomes

$$\tilde{\sigma}_{zz}^1 = \sum_{n=1}^{\infty} \sum_{i=1}^{3} (-1)^n \left(n\pi\gamma_i \right)^2 \left(c_{13} - \frac{c_{33} l_{1i}}{(\gamma_i)^2} - \frac{e_{33} l_{2i}}{(\gamma_i)^2} \right) \left(c_{I00} + \sum_{j=1}^{\infty} c_{I0i} J_0(\xi_j r) \right) A_{in} \tag{17}$$

Similarly, series expansion for matching the functions can be applied to other mechanical and electrical boundary conditions. After considering all boundary conditions given by Equation (10), an equation system of order $6M + 3$ can be established, where M is the total number of terms used in the series expansion. This system can be solved numerically to determine all remaining unknown arbitrary functions appearing in the general solutions in Equations (9a)-(9c). Once all unknowns are determined, an efficient numerical scheme is employed to perform Laplace inversion to obtain all field quantities in the time domain.

Numerical Results and Discussion

A selected set of numerical solutions is presented in this section to demonstrate the basic features of coupled thermo-electro-mechanical fields corresponding to the problem shown in Figure 1. The computation of thermopiezoelectric cylinder solutions involves the numerical evaluation of finite integrals and Laplace inversion to obtain time domain solutions. The numerical integrations are performed by using quadrature integration scheme. For the present class of problems, numerical Laplace inversion can be performed

very accurately by using a scheme proposed by Stehfest [14]. The formula due to Stehfest is given by

$$f(t) \approx \frac{\log 2}{t} \sum_{n=1}^{N} c_n \tilde{f}\left(n \frac{\log 2}{t}\right) \tag{18a}$$

where

$$c_n = (-1)^{n+N/2} \sum_{k=\lfloor (n+1)/2 \rfloor}^{\min(n, N/2)} \frac{k^{N/2}(2k)!}{(N/2-k)!k!(k-1)!(n-k)!(2k-n)!}, \quad N \text{ is even} \tag{18b}$$

Table 1. A Convergence Study with Respect to the Numbers *N* Given in Equation (18) for Solutions of Nondimensional Temperature Distribution in an Infinite Solid Elastic Cylinder [15]

r/h	Present Study				Carslaw& Jaeger [15]
	***N* = 8**	***N* = 10**	***N* = 12**	***N* = 14**	
0.01	0.0148	0.0159	0.0161	0.0161	0.0161
0.40	0.0948	0.0943	0.0941	0.0941	0.0941
0.70	0.4139	0.4143	0.4143	0.4143	0.4143

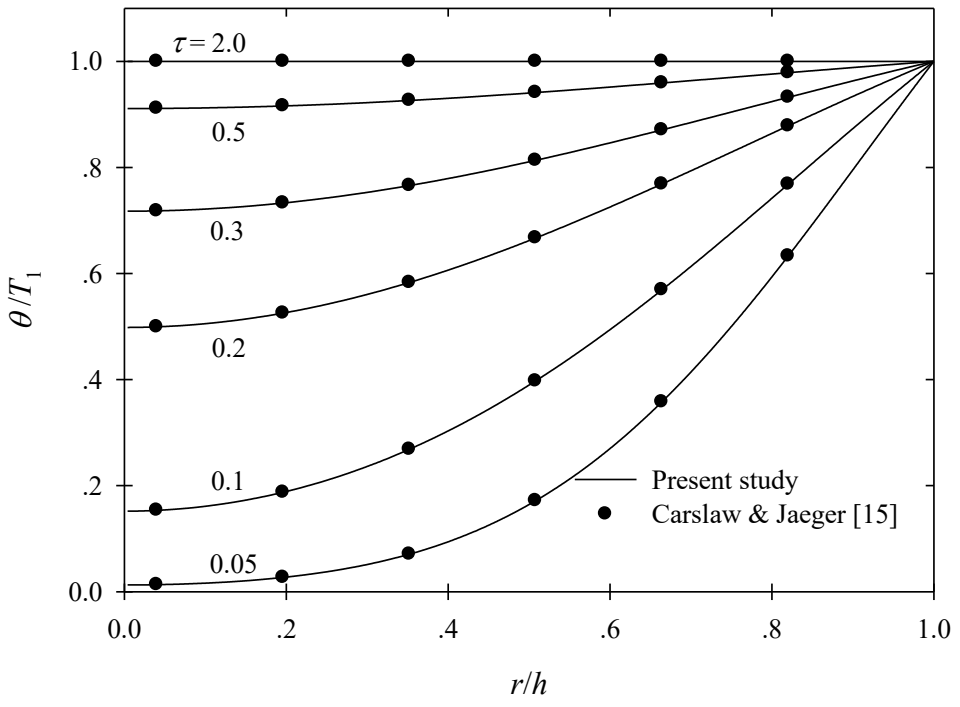

Figure 2**.** Comparison of temperature distribution in an infinite solid elastic cylinder [15].

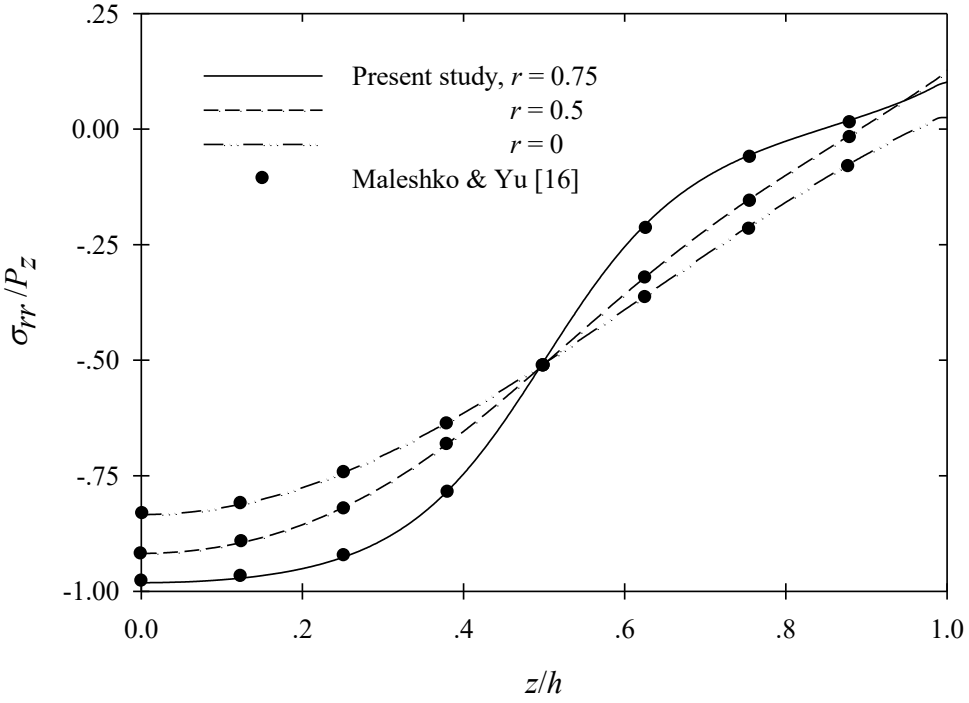

Figure 3**.** Comparison of radial stresses for a finite solid cylinder subjected to discontinuous normal loading [16].

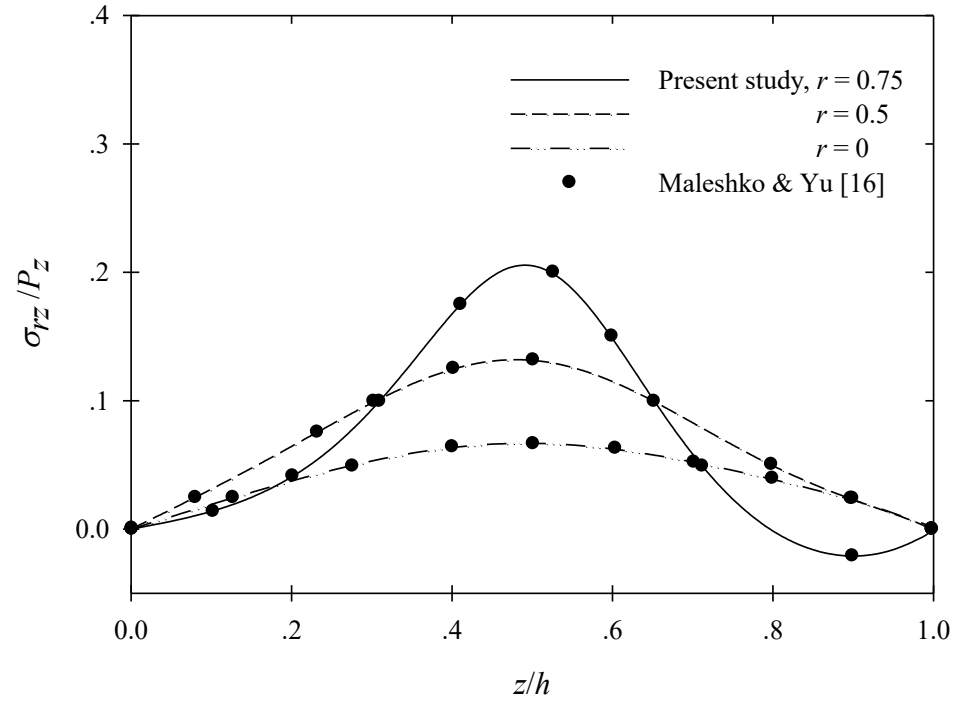

Figure 4**.** Comparison of tangential stresses for a finite solid cylinder subjected to discontinuous normal loading [16].

The accuracy of the present solution scheme is first verified by comparing with existing solutions available in the literature. A nondimensional time defined as $\tau = \kappa t / a^2$ is used in the numerical study, where κ and a denote thermal diffusivity and radius of solid cylinder respectively. Table 1 presents a convergence study with respect to the number N given in Equation (18) for nondimensional temperature (θ/T_1) in an infinitely long elastic cylinder where T_1 is the p rescribed uniform temperature at the lateral surface of the cylinder. The present temperature solutions are obtained by using different values of N at $\tau = 0.1$. Existing solutions given by Carslaw and Jaeger [15] are also presented for comparison. Numerical results presented in Table 1 indicate that the present solution can be obtained very accurately with $N \geq 12$. A convergence study of the number of terms used in the series expansion, M, was also investigated. It was found that numerically stable and converged solutions can be obtained by using the number of series terms $M \geq 15$. All numerical results presented in this paper, unless otherwise specified, correspond to the case where $N = 12$ and $M = 15$.

Comparison of the nondimensional temperature of an infinite elastic cylinder [15] is presented in Figure 2 at different nondimensional time τ = 0.05, 0.1, 0.2, 0.3, 0.5 and 2.0. It can be observed that the present solutions agree very closely with the results given by Carslaw and Jaeger [15]. Figures 3 and 4 present comparisons of radial and tangential stresses for a finite solid elastic cylinder, with $h = a$ and Poisson"s ratio of $1/3$, subjected to discontinuous normal loading on lateral surface between the present solutions and those given by Meleshko and Yu [16]. The loading function applied at the lateral surface of the cylinder is defined by

$$P(z) = \begin{cases} -P_z, & |z| \leq h/2 \\ 0, & h/2 < |z| \leq h \end{cases} \tag{19}$$

Solutions of an elastic cylinder can be obtained from the present scheme by setting the piezoelectric coefficients to negligibly small values. It can be seen from Figures 3 and 4 that the present solutions are in excellent agreement with those given by Meleshko and Yu [16].

Table 2. Material Properties Used in the Numerical Study

Coefficients	Piezoelectric Materials		
	CdSe	PZT–6B	PZT–4
($10^{10} N/m^2$)	7.41	16.8	13.9
($10^{10} N/m^2$)	8.36	16.3	11.5
($10^{10} N/m^2$)	4.52	6.0	7.78
($10^{10} N/m^2$)	3.93	6.0	7.43
($10^{10} N/m^2$)	1.32	2.71	2.56
(C/m^2)	-0.16	-0.9	-5.2
(C/m^2)	0.347	7.1	15.1
(C/m^2)	-0.138	4.6	12.7
($10^{-9} F/m$)	0.826	3.6	6.45
($10^{-9} F/m$)	0.903	3.4	5.62

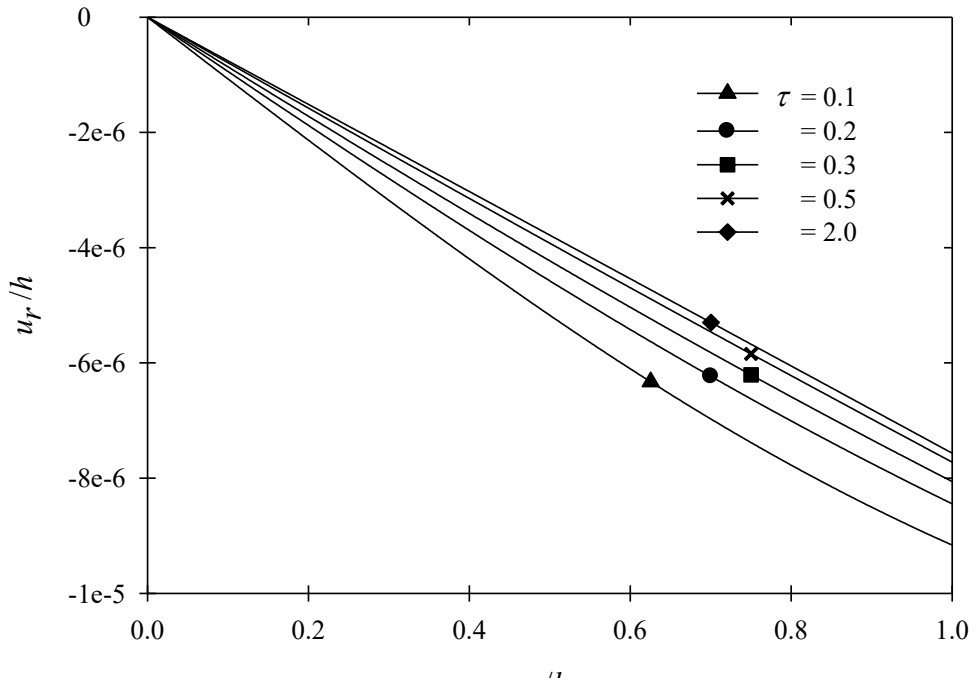

Figure 5. Radial displacement of finite solid CdSe cylinder due to constant temperature and mechanical loading ($z = 0$).

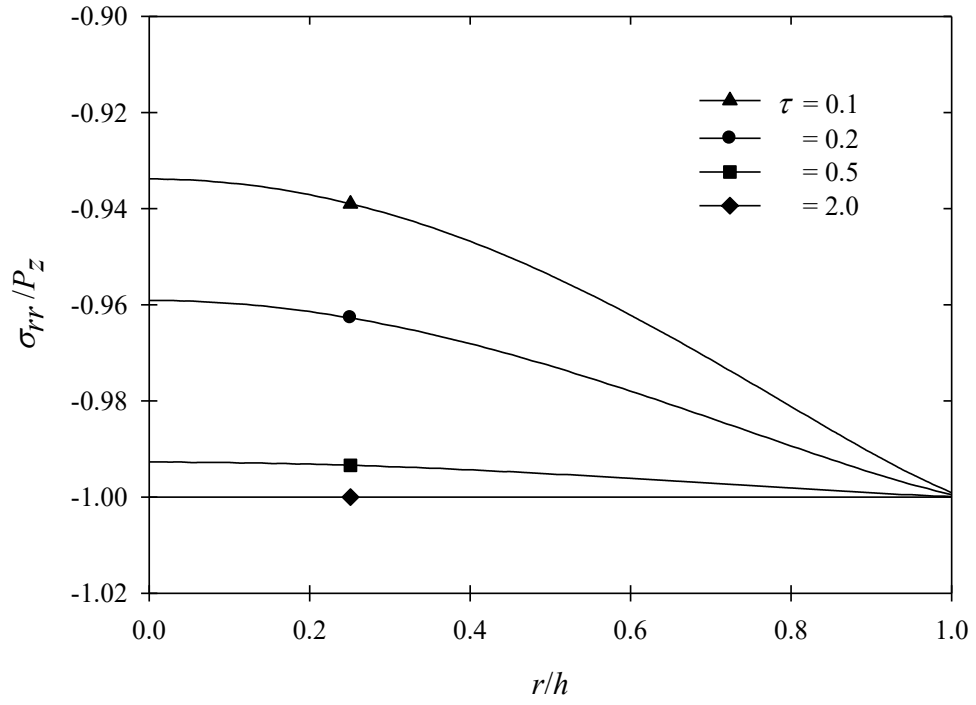

Figure 6. Radial stress of finite solid CdSe cylinder due to constant temperature and mechanical loading ($z = 0$).

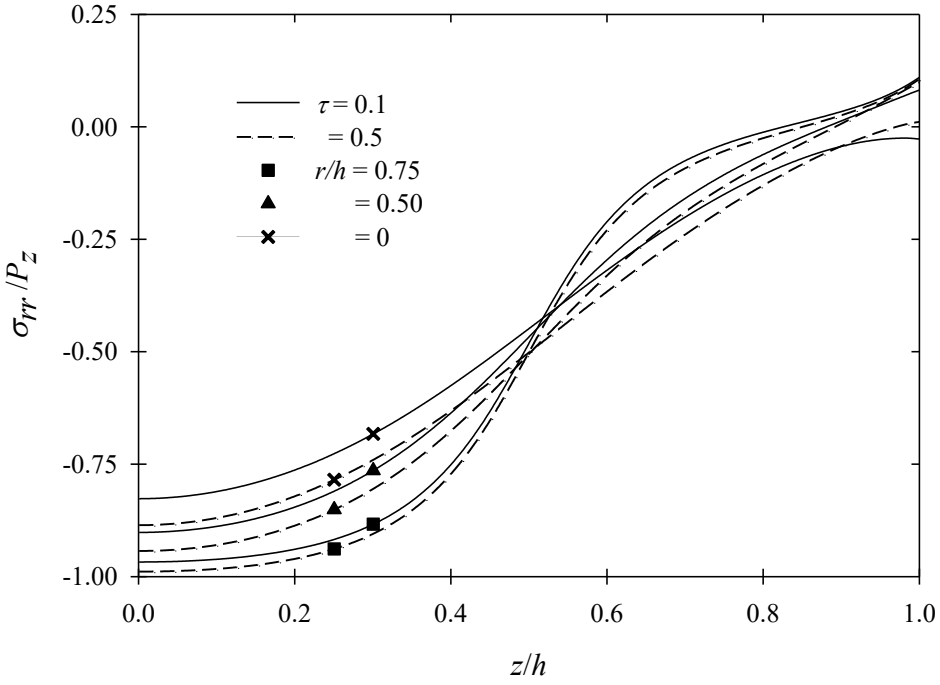

Figure 7**.** Radial stress along z-direction due to uniform temperature and banded mechanical loading (CdSe, $h_0 = h/2$, $a/h = 1$).

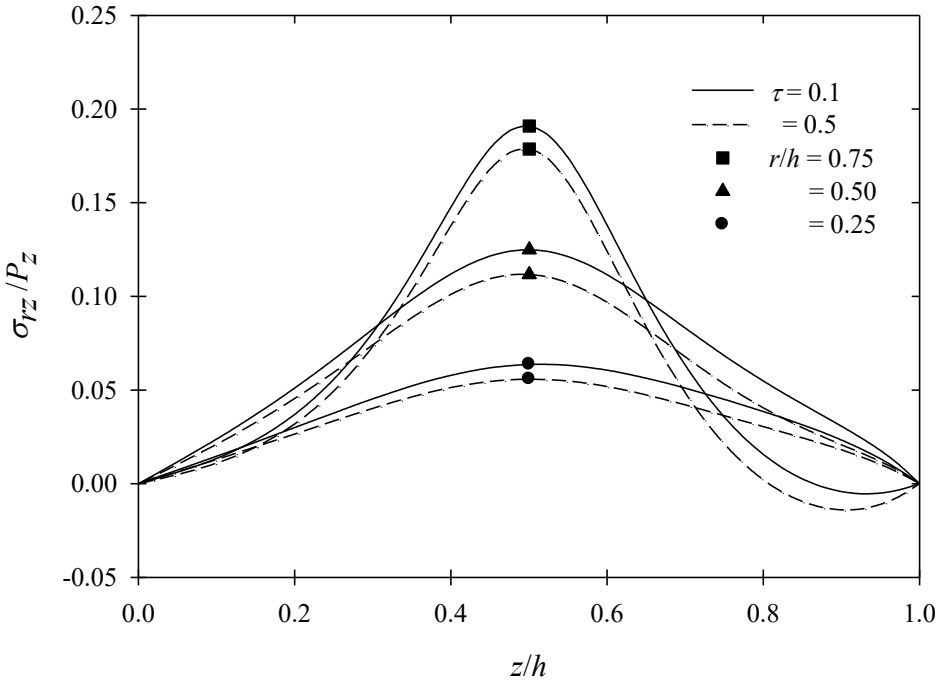

Figure 8**.** Shear stress along z-direction due to uniform temperature and banded mechanical loading (CdSe, $h_0 = h/2$, $a/h = 1$).

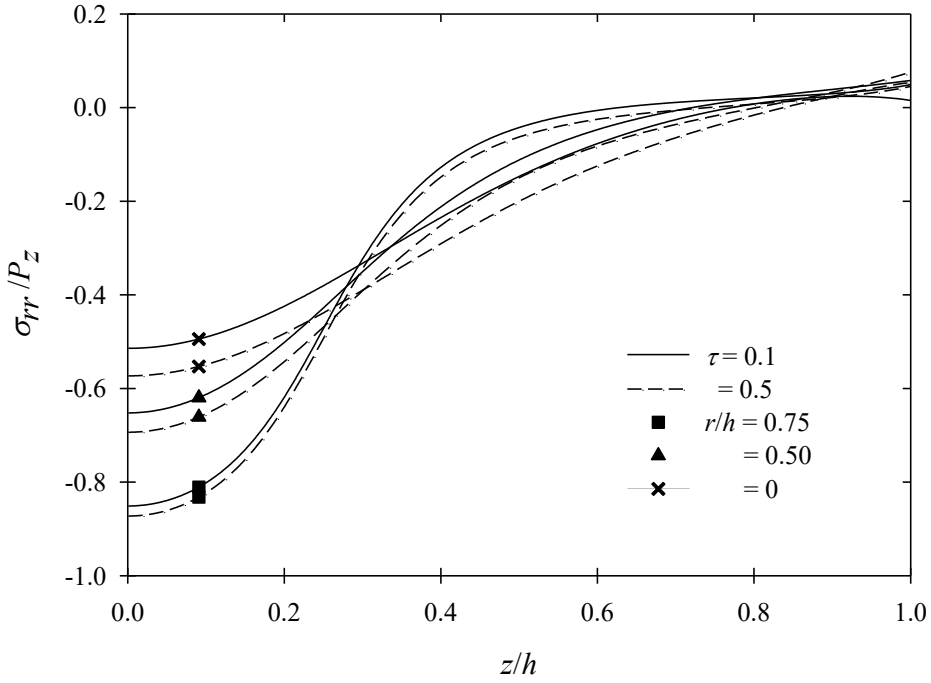

Figure 9**.** Radial stress along z-direction due to uniform temperature and banded mechanical loading (CdSe, $h_0 = h/4$, $a/h = 1$).

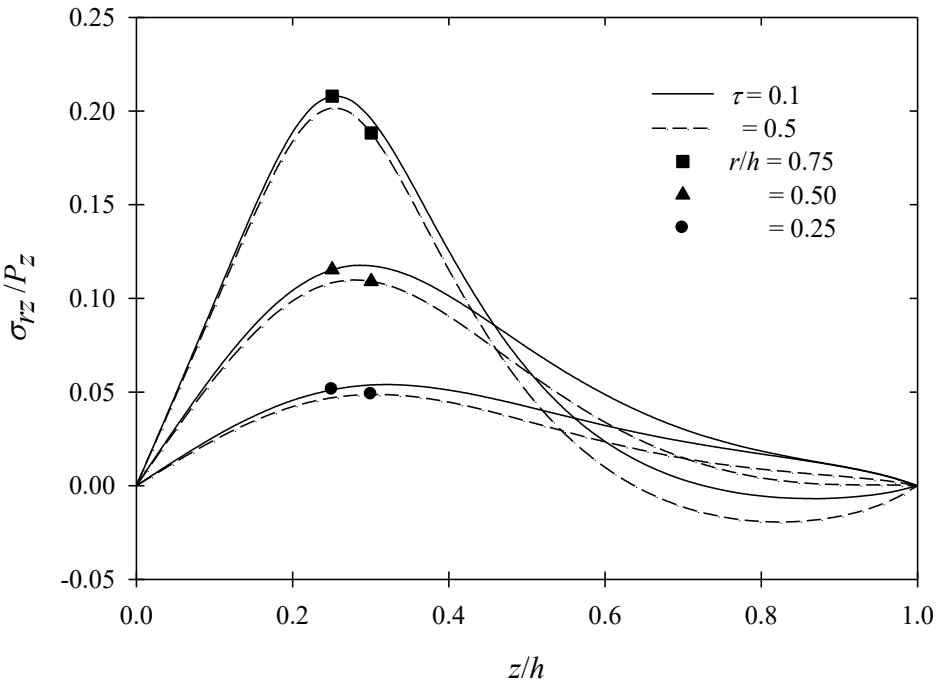

Figure 10**.** Shear stress along z-direction due to uniform temperature and banded mechanical loading (CdSe, $h_0 = h/4$, $a/h = 1$).

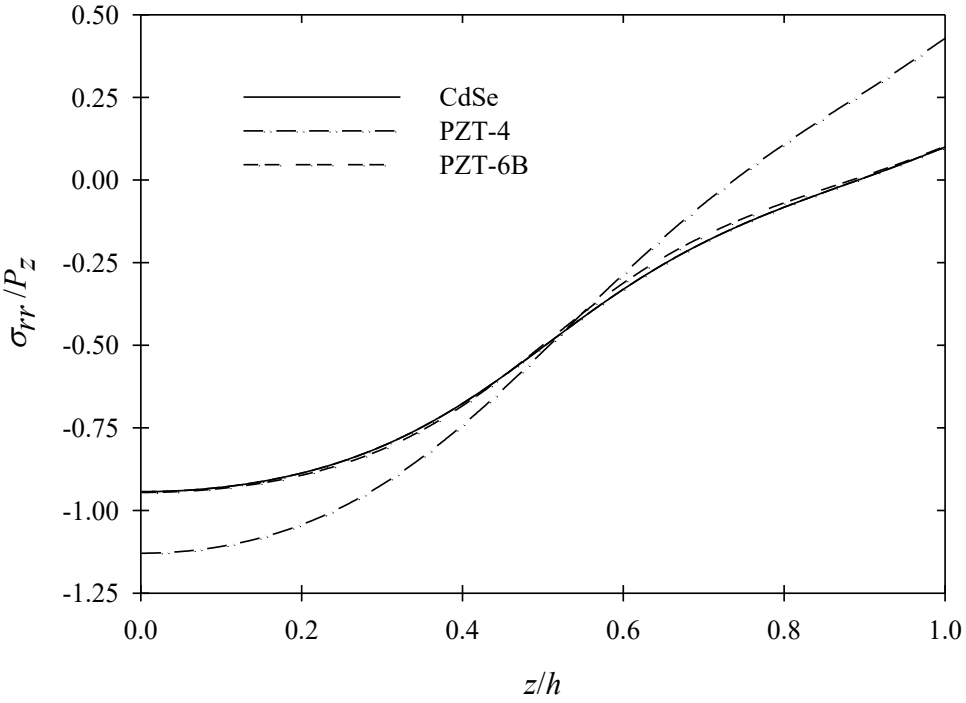

Figure 11. Radial stress along the z-direction due to uniform temperature and banded mechanical loading ($h_0 = h/2$, $a/h = 1$).

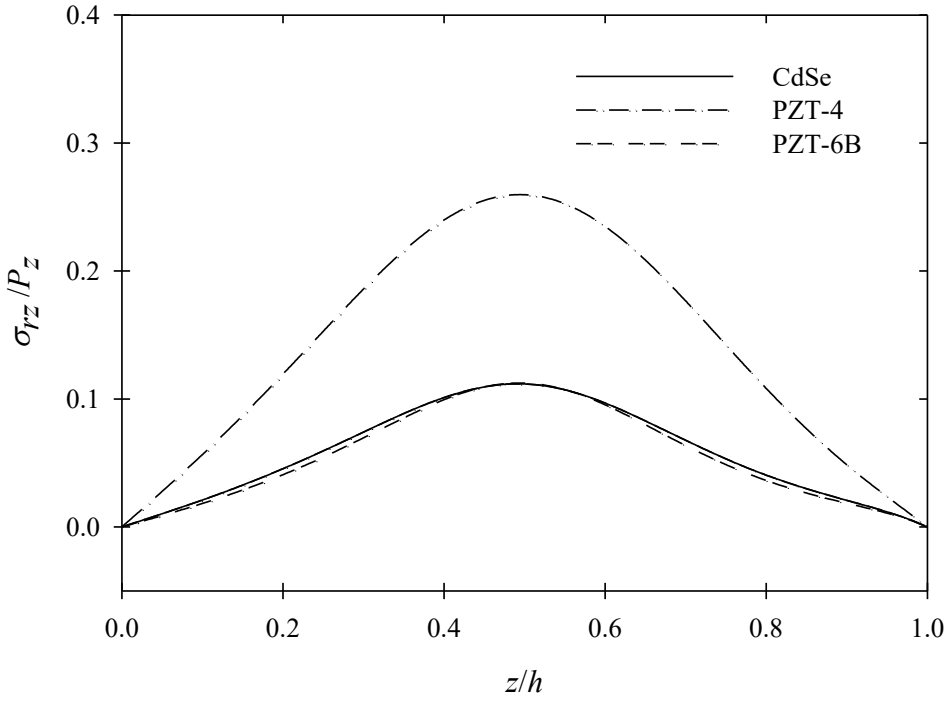

Figure 12. Tangential stress along the z-direction due to uniform temperature and banded mechanical loading ($h_0 = h/2$, $a/h = 1$).

Selected numerical solutions for finite solid thermopiezoelectric cylinder as shown in Figure 1 are presented next to portray the salient features of themopiezoelectric responses for a piezoelectric finite cylinder under thermoelectromechanical loading. All numerical results presented hereafter correspond to cases where uniform temperature $\theta(t) = T_1 H(t)$ and radial traction $\sigma_{rr} = P_z H(t)$, where T_1 and P_z are constants, are simultaneously applied over an outer lateral surface of a thermopiezoelectric cylinder with $h = a$. Piezoelectric material properties used in the numerical study are given in Table 2.

Figures 5 and 6 show radial displacements and radial stresses on the $z = 0$ plane in the r-direction respectively for a finite solid cylinder made of Cadmium Selenide (CdSe). It can be seen from Figures 5 and 6 that the radial displacement and radial stress of the cylinder are varied with time before reaching the steady state condition when $\tau = 2$. Radial displacements due to applied traction and temperature change are almost linear with respect to the radial axis. At the steady state, thermal stress (stress due to non-uniform distribution of temperature) is disappeared and hence stresses in the cylinder are solely due to the applied traction. The deformations of the cylinder at the steady state are, however, influenced by both temperature change and mechanical loading.

Next, the case of a thermopiezoelectric finite cylinder of CdSe subjected to banded radial traction under uniform temperature is considered. The function of banded mechanical loading is given by

$$\bar{P}(z,t) = \begin{cases} -P_z H(t), & |z| \le h_0 \\ 0, & h_0 < |z| \le h \end{cases} \tag{20}$$

Two cases of banded mechanical loading are considered in the numerical study, i.e., $h_0 = h/2$ in Figures 7 and 8, $h_0 = h/4$ in Figures 9 and 10 respectively. Under this loading case, larger number of series for converged solutions is required, i.e. $M \ge 50$. The numerical results are presented for various radial distances, r/h, at different nondimensional times, τ, to show stress distributions along the vertical direction in thermopiezoelectric cylinders at transient state. The numerical results presented in Figures 7-10 reveal non-uniform distribution of radial and shear stresses along the z-direction. Similar trends of stress distribution are observed from both loading cases at all presented radial distances. The maximum radial and shear stresses are found at $r/h = 0.75$. In addition, the magnitudes of radial stresses for the case $h_0 = h/2$ are evidently higher than those of $h_0 = h/4$, whereas the maximum shear stresses generated in thermopiezoelectric cylinders under $h_0 = h/2$ and $h_0 = h/4$ are not significantly different.

Figures 11 and 12 show radial and tangential stresses respectively for a finite thermopiezoelectric solid cylinder subjected to uniform temperature and banded mechanical loading ($h_0 = h/2$). The numerical results are presented in Figures11 and 12 for three different types of piezoelectric materials, namely, CdSe, PZT-4 and PZT-6B (see Table 2) and $\tau = 2$. It can be seen from numerical results in Figures 11 and 12 that the material properties have a significantly influence on the cylinder responses. In particular, stresses in PZT-4 cylinder are generally higher than those of CdSe and PZT-6B cylinders.

Conclusions

In this paper, a comprehensive analysis of a finite thermopiezoelectric solid cylinder under axisymmetric electromechanical and thermal loading is presented. The formulation of a boundary-value problem is based on general solutions of a thermopiezoelectric cylinder, which are derived by employing a generalized displacement potential function method together with a Fourier-Bessel series expansion. Current numerical solutions agree well

with the existing solutions for the limiting case of a thermoelastic cylinder. Numerical results of a finite solid thermopiezoelectric cylinder are shown for different loading conditions and material types. The present general solution, and the analytical procedure outlined in this paper can be further extended to solve more complicated boundary-value problems involving finite hollow cylinders and composite cylinders.

Acknowledgement

The work presented in this paper was supported by a research grant under the National Research University Project (NRU-CU: Grant No. AM1011A). This support is gratefully acknowledged.

References

[1] K. Uchino, "Materials issues in design and performances of piezoelectric actuators: An overview," *Acta Materialia*, Vol. 46, pp. 3745–3753, 1998.

[2] S.S. Rao, and M. Sunar, "Piezoelectricity and its use in disturbance sensing and control of flexible structures: A survey," *Applied Mechanics Reviews*, Vol. 47, pp. 113–123, 1994.

[3] R.D. Mindlin,"Coupled piezoelectric vibrations of quartz plates," *International Journal of Solids and Structures*, Vol. 10, pp. 453-459, 1974.

[4] P.J. Chen, "Three–dimensional dynamic electromechanical constitutive relations for ferroelectric materials," *International Journal of Solids and Structures*, Vol. 16, pp. 1059–1067, 1980.

[5] W.F. Deeg, *The Analysis of Dislocation, Crack and Inclusion Problems in Piezoelectric Solids*, Thesis (PhD), Stanford University, 1980.

[6] V.Z. Parton, and B.A. Kudryavtsev, *Electromagnetoelasticity*, Gordon and Breach, New York, 1988.

[7] R.K.N.D. Rajapakse, and Y. Zhou, "Stress analysis of piezoceramic cylinders," *Smart Materials and Structures*, Vol. 6, pp. 169-177, 1997.

[8] R.K.N.D. Rajapakse, T. Senjuntichai, and W. Kaewjuea "Piezoelectric cylinder under voltage and axial loading," *International Journal of Applied Electromagnetics and Mechanics*, Vol. 27, pp. 93–116, 2008.

[9] F. Ashida, and T.R. Tauchert, "Transient response of a piezothermoeleastic circular disk under axisymmetric heating," *Acta Mechanica*, Vol. 128, pp. 1-14, 1998.

[10] Y. Tanigawa, and Y. Ootao, "Transient piezothermoelectric of a two layered composite hollow cylinder constructed of isotopic elastic and piezoelectric layers due to asymmetrical heating," *Journal of Thermal Stress*, Vol. 30, No. 9-10, pp. 1003-1023, 2007.

[11] T. Ikeda, *Fundamentals of Piezoelectricity*, Oxford University Press, New York, 1996.

[12] I.N. Sneddon, *Fourier Transforms*, McGraw-Hill, New York, 1951.

[13] G.N. Watson, *A Treatise on the Theory of Bessel function*, Cambridge University Press, England, 1962.

[14] H. Stehfest, "Numerical inversion of Laplace transform," *Communications of the ACM*, Vol. 13, pp. 47-49, 1970.

[15] H.S. Carslaw, and J.C. Jaeger, *Conduction of Heat in Solids*, 2nd Edition, Oxford University Press, England, 1959.

[16] V.T. Yu, and V.V. Meleshko, "Equilibrium of an elastic finite cylinder under axisymmetric discontinuous normal loadings," *Journal of Engineering Mathematics*, Vol. 78, pp. 143-166, 2013.